Towards Practical Path Loss Predictions in Indoor Corridors Considering 5G mmWave Three-Dimensional Measurements

Melissa Eugenia Diago-Mosquera, Alejandro Aragón-Zavala, *Senior Member, IEEE*, and Mauricio Rodriguez, *Senior Member, IEEE*

***Abstract*—Theoretical and empirical foundations of how radio waves behave in practical wireless channels need to be fully revisited for millimeter-wave (mmWave) frequencies so that fifth-generation (5G) technologies may be successful. Kriging is an outstanding geostatistal interpolation technique that employs variography to understand the spatial variability of known samples at specific locations to predict unmeasured samples, based on the fact that there is an implied connection between the measured value and its location in space. The research we here report is aimed at validating the improvement in predictions when this tool is included for mmWave frequency path loss modeling in a long indoor corridor with break. In order to quantify the accuracy of the proposed methodology, it is compared with a well-established procedure described in the literature. Extensive path-loss measurements were collected through specialized narrowband sounders at 28 and 60 GHz. Spatially averaged power measurements using omnidirectional and directive antennas at different heights provided the empirical basis for the three-dimensional Kriging-aided model. It was found that this method significantly improves the accuracy as it considers all the singularities and site-associated features that are implicit in measured samples. This is important to obtain a reliable path loss model for planning and deployment of mmWave wireless communication systems in indoor scenarios.**

***Index Terms*—Fifth-generation (5G) mmWave, indoor corridor, Kriging, path loss model.**

I. Introduction

AS PROMISED by the fifth generation (5G) of radio communication networks, future wireless mobile systems will be inclusive, i.e., technologies for supporting wireless connectivity for any rates, type of communicating units, and scenarios [1]. To meet this ambitious aim, reliable path loss modeling for millimeter-wave (mmWave) frequencies is essential to provide accurate predictions for the deployment of 5G wireless service. These services are likely to be extensively used in indoor environments such as office spaces linked by long corridors. Propagation in corridors, whose structural geometry resembles a waveguide, has been reported to exhibit path losses lower than those observed in free space, attributable to the contributions of reflections along walls, floor, and ceiling. This has been referred to in the literature as *"waveguide effect"* [2]–[5], characterized by a path loss exponent (PLE) less than 2, as reported in [6].

Path loss models for indoor corridors at various frequencies have been reported in several previous studies. The model derived in [7] is easy to implement and has clear physical meaning for line-of-sight (LOS) in indoor corridors at 5.25 GHz. Batalha *et al.* [8] employed measurements to adjust path loss prediction models of radio propagation for indoor environments in the frequency band of 8 to 11 GHz. However, these studies have not explicitly discussed waveguiding, which is the reason for a PLE less than 2. Other research, such as those reported in [9], have included this effect through a modified method named effective wall loss model to estimate the path loss at 2.4, 5.3, 28, 60, and 73.5 GHz. In [10], motivated by the waveguiding effect, the authors have proposed a single-slope segmentwise path gain model for transmission along corridors at 28 GHz. In [11], to overcome channel complexity and time-consuming measurements, a novel methodology using an artificial neural network techniques in indoor corridors at 3.7 and 28 GHz has been studied. To improve path loss models for indoor corridors, in [12], the close-in free-space reference distance model and the floating-intercept model were studied and optimized considering 14, 18, and 22 GHz measurements. In total, 14 and 22 GHz were also considered in [5] where a dual slope large-scale path loss model was evaluated. Propagation measurements at 26 and 38 GHz have been conducted in [13] to investigate propagation characteristics of indoor corridors. Even though the works presented in [5] and [7]–[13] were suitable to predict path loss in indoor corridors, their validation was restricted to two-dimensional (2-D) since their models only accounted for one receiver height without considering the complete coverage in a three-dimensional (3-D) space.

Generally, for radio propagation predictions path loss has been modeled using the log-distance model, which includes normal distributed shadow fading [14], [15]. Other studies have taken advantage of the spatial correlation of shadowing to estimate it by including Kriging, which has minimized the variance of estimation errors, due to Kriging employs variography to restrict how far and where to look for the samples to be used in the

Manuscript received 9 June 2022; revised 30 June 2022; accepted 9 July 2022. Date of publication 12 July 2022; date of current version 6 October 2022. This work was supported in part by the National Council of Science and Technology CONACYT through the student scholarship 746015; in part by the Chilean Research Agency ANID under Grants ANID FONDECYT 1211368, ANID FONDEQUIP EQM190023, and ANID PIA/APOYO AFB180002; and in part by the Project VRIEA-PUCV 039.437/2020. *(Corresponding author: Melissa Eugenia Diago-Mosquera.)*

Melissa Eugenia Diago-Mosquera and Alejandro Aragón-Zavala are with the Escuela de Ingeniería y Ciencias, Tecnologico de Monterrey, Querétaro 76130, Mexico (e-mail: a00829220@tec.mx; aaragon@tec.mx).

Mauricio Rodriguez is with the Escuela de Ingeniería Eléctrica, Pontificia Universidad Católica de Valparaíso, Valparaíso 2362804, Chile (e-mail: mauricio.rodriguez.g@pucv.cl).

Digital Object Identifier 10.1109/LAWP.2022.3190324

Fig. 1. Equipment and scenario. (a) Receiver system platform at 60 GHz. (b) Long corridor at the USM with break.

interpolation [16], yielding accurate shadowing predictions, as has been validated in [17] and [18]. However, these models have not considered the 3-D propagation geometry to predict the path loss at mmWave frequencies nor employed Kriging to estimate path loss.

The principal novelty in the work here reported is the inclusion of Kriging as an effective tool to improve modeling accuracy for mmWave indoor propagation as it considers all the singularities and site-associated features that are implicit in measured samples. To the best of our knowledge this has not been reported before despite the fact that its potential has been validated [19]–[21] in previous work. Therefore, this letter is focused on better understanding and modeling path loss considering long indoor corridors, the effect of corners and different receiver heights (i.e., 3-D) validating the benefits of using Kriging to ensure accurate path loss predictions.

II. Measurement Campaigns and Data Collection Procedure

A detailed description of the radio measurements conducted in typical indoor corridor scenarios is provided as follows.

A. Measurement Equipment

Universidad Técnica Federico Santa María (USM) in collaboration with Pontificia Universidad Católica de Valparaíso (PUCV) and Nokia Bell Laboratories constructed two narrowband sounders at 28 GHz [10] and 60 GHz.

The sounders transmit a—22.5 dBm at 28 GHz and 20.5 dBm at 60 GHz—continuous wave tone into vertically polarized horn antennas with 55° half-power beamwidths (HPBWs) and 10 dBi of gain. In both cases, the power is recorded by narrowband receivers with the alternative of using horn and omnidirectional (omni) antennas. For 28 GHz the omni antenna has a 1.4 dBi gain. The horn antenna has a 25 dBi gain and 10° HPBWs. At 60 GHz the omni antenna has a 2 dBi gain and a vertical HPBW of 30°. The horn antenna has 25 dBi of gain and 9° HPBW in the E-plane and 10° HPBW in the H-plane. The receiver is shown in Fig. 1(a).

The received signal is amplified by several adjustable gain low-noise amplifiers, mixed with a local oscillator and narrowband filtered at a 100 MHz intermediate frequency. A logarithmic-gain power meter generates 740 samples/second, which are transmitted to a laptop computer. The receiver is placed on a rotating 360° platform with the horn antenna rotating on its phase center and the omni antenna describing a circle of 20 cm radius. The path loss is calculated based on the spatially averaged power measurements received at each location. Average power received by rotating the horn antenna is equivalent to spatial averaging of the omni antenna after compensating for elevation gain if all received multipath wavefronts are within the vertical beamwidth of either antenna, according to the radiation pattern analysis [10]. Using both types of antennas allowed us to verify if there is a significant contribution of received power that the narrower vertical-beamwidth horn antenna will miss.

B. Experimental Scenario and Data Acquisition

In order to represent typical long indoor corridors, received signal-strength measurements were carried out in a long corridor with one 90° break at 37 m from the transmitting antenna—dividing corridor A from corridor B, Fig. 1(b)—in the engineering school of the USM. Corridor A is 39 m long, 3.6 m high, and 2.74 m in width. Corridor B is 16 m long, 3.7 m high, and in 2.57 m width. Both corridors are lined with rooms. The walls and ceilings consist of brick and concrete, with a ceramic-tile floor. At 28 m from the transmitter position, there is a glass door with aluminum frame. The transmitter was always placed in the middle of the corridor at a 1.66 m height and the horn antenna of the transmitter system was manually aimed to get maximum averaged received power at the measured locations.

The first measurement was recorded at 2 m from the transmitter and subsequent samples were spaced every 1 m, resulting in 37 measurements for corridor A and 16 for corridor B, yielding 53 measurements for each system configuration, obtained when varying: 1) frequency, 28 and 60 GHz; 2) type of receiver antenna, horn and omni; 3) receiving height, 0.98 (h_1), 1.66 (h_2), and 2.03 m (h_3). Consequently, a total of 636 radio measurements were made.

Propagation in this scenario can be classified into two types of links: LOS, corridor A, and non-line-of-sight (NLOS), corridor B. NLOS results from reflected, dispersed, and/or diffracted paths after the break. For the sampling process the receiver platform is programed to switch every ten turns between omnidirectional and horn antenna. This is done for 30 s with the platform rotating at 100 r/min. Small-scale fades are eliminated by averaging power over all angular positions for both types of antennas. Average power over successive rotations is compared to assure consistency in a static environment where no significant temporal variation is to be expected. This sampling process resulted in 636 links. The corresponding path losses are illustrated in Fig. 2, where as expected, we found that the spatially averaged path losses are very close for both types of antennas. This is further discussed in Section IV.

III. Channel Modeling

As a benchmark for comparison to our results we use the most accurate single-slope segmentwise model presented in [10], for the specific case of one break, i.e., one LOS corridor followed by a 90° break and a NLOS corridor. This is described by

$$\hat{L} = \begin{cases} L(d_0) + 10n \log d, & \text{LOS} \\ L(d_0) - S + 10n \log\left(x_1\left(d - x_1\right)\right), & \text{NLOS} \end{cases} \quad (1)$$

where $L(d_0)$ is the free-space path loss at the reference distance $d_0 = 1\text{m}$, n is the path loss exponent, d is the "Manhattan distance" of the path, i.e., the sum of the path lengths along the corridors from the transmitter to the receiver, S is the around-the-corner loss, and x_1 is the length of the LOS segment, 37 m after which the transition to NLOS causes an evident increase

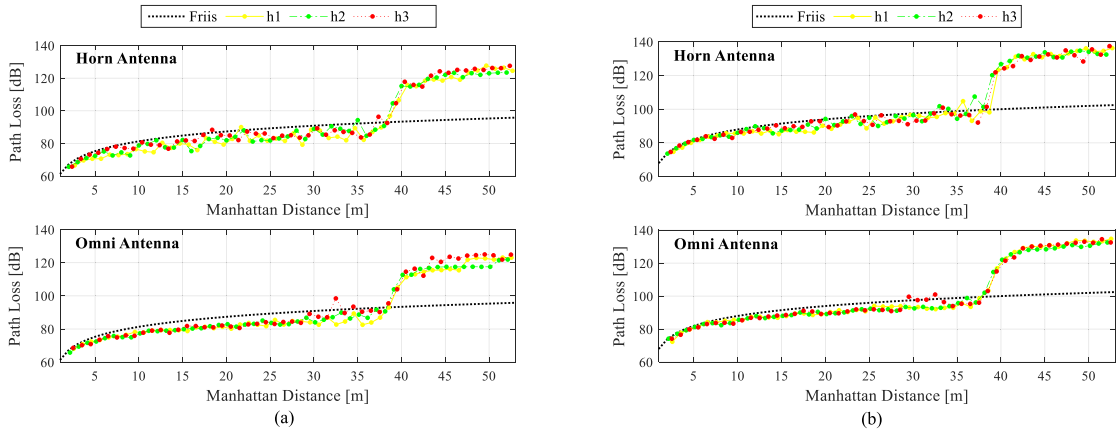

Fig. 2. Path loss measured at three-receiver heights. (a) 28 GHz. (b) 60 GHz.

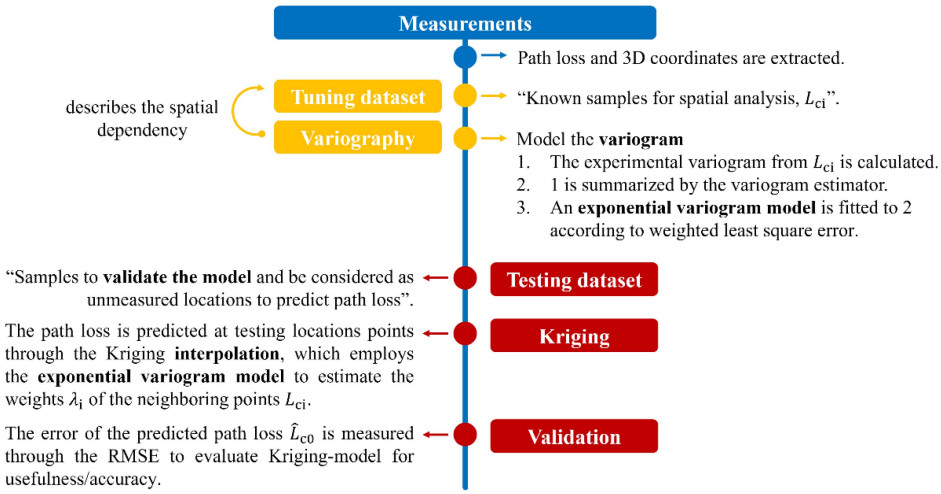

Fig. 3. Methodology for the Kriging-aided path loss predictions.

in path loss as seen in Fig. 2. The values of n and S are fitted from measurements according to the best fit of a classical linear regression.

Based on the fact that the closest samples to the unmeasured locations have the most influence, Kriging predicts path loss values at an unmeasured location with c0 3-D coordinates, forming weights λ_i based on surrounding measured path loss L_{ci}, at known locations with ci 3-D coordinates, following the methodology described in Fig. 3. The path loss proposed is modeled as

$$\hat{L}_{c0} = \sum_{i=1}^{N(h)} \lambda_i L_{ci} \tag{2}$$

where $N(h)$ is the number of known measured pairs within the lag interval h, i.e., for the variography, the distance separation between all measured locations is computed to select neighbor samples by restricting how far (maximum lags) and where to look (in each lag) for the samples to be used in the interpolation through a matrix of Euclidean separation distances. This procedure is described in more detail in [22]. In (2), h is calculated as the mean of the minimum separation distance and $N(h)$ is the resulting number of pairs with h as the separation distance. An extended explanation of the process to form the λ_i weights to interpolate and predict unmeasured values can be found in [17].

IV. Results

The proposed mathematical model in (2) takes advantage of the spatial analysis of measured samples included in the variography process, which generates the principal boundary that Kriging considers for interpolations. The results we here present are aimed at two distinct objectives, first quantifying the benefit of including 3-D measurements and second, assessing the advantage of using the Kriging-aided model (2). To this effect, three different cases to select tuning and testing datasets are considered. A tuning dataset is used to train the models, in order to fit n and S in (1) and model the variogram to estimate λ_i in (2). The testing dataset allows us to predict the path loss when using the previously obtained model at the 3-D locations and compare them to the measured values. The first case aims to analyze the accuracy of the predictions at heights h_3 and h_1, i.e., higher and lower than the transmitter antenna when the models are tuned using only measurements at the same transmitter height, h_2; The second case uses the samples at h_1 and h_3 to tune and test the models, from each height. In total, 60% of data is randomly selected for the tuning dataset and the remaining 40% from each

TABLE I
RESULTS FOR PATH LOSS PREDICTIONS EMPLOYING (1) AND (2)

Frequency [GHz]	Receiver Antenna	Case	n	S [dB]	RMSE_1 [dB]	RMSE_K [dB]
28	Horn	1	1.77	-15.0	3.6	3.1
		2	1.70	-18.1	3.6	2.9
		3	1.73	-17.1	3.6	3.0
	Omni	1	1.68	-15.3	2.9	2.4
		2	1.70	-15.9	3.0	2.1
		3	1.69	-15.7	2.9	2.0
	all cases		1.71	-16.2	3.2	2.6
60	Horn	1	2.00	-14.0	3.9	2.9
		2	1.87	-16.9	3.8	3.0
		3	1.91	-16.0	3.6	2.9
	Omni	1	1.78	-16.5	2.5	2.0
		2	1.82	-16.9	2.7	1.6
		3	1.81	-16.8	2.5	1.6
	all cases		1.87	-16.2	3.2	2.3
			averaged RMSE		3.2	2.5

height for the testing dataset. Finally, the third case tunes/tests the models considering a rate of 60/40 percentage randomly selected from the samples measured at each of the three-heights: h_1, h_2, and h_3.

The accuracy and effectiveness of the predictions achieved with (2) are evaluated and compared against those calculated with (1) through the root-mean-square error (RMSE) metric considering all the three cases described. In Table I, the fitted values, n and S, are calculated with (1), RMSE_1 refers to the RMSE calculated when (1) is employed, and RMSE_K when (2) is used to predict the path loss at testing locations. These parameters depend on the specific case selected to tune/test (1) and (2), therefore, in Table I, the column "case" is included.

To analyze the results, it is important to bear in mind that the first case considers only same-height transmit and receive measurements for tuning, so the possible effect of dissimilar heights is not part of the model. Instead for the second and third cases possible 3-D effects are included, as transmitter and receiver are at different heights. For the second and third cases, the 60/40 rate is based on random sample selection, therefore, the variability of the tuning/testing dataset must be considered. Thus, 2000 iterations with a 60/40 rate were assessed to quantify n, S, and the RMSE. The results in Table I correspond to the average over the 2000 iterations, in contrast to the first case where all samples were used to obtain a single value. In order to overview the results listed for the horn and omni antennas at both frequencies, the values of n, S, RMSE_1, and RMSE_K are averaged and referred to as *all cases* in Table I. Also, the RMSE reported for *all cases* is averaged and listed at the end of Table I.

Table I, first, shows that both type of antennas yields very similar path loss parameters indicating that virtually all power is collected by the narrower vertical-beam horn antenna, i.e., most multipath wavefronts are close to the horizontal plane. We also note that the omni antenna measurements have a consistently lower RMSE. This suggests that although the omni antenna moves over a relatively short range this nevertheless contributes to reducing the shadowing that can affect the horn, which only spins on axis with no displacement.

As seen for both types of antennas at 28 and 60 GHz n was less than 2, suggesting a better scenario than free space, which is the effect of waveguiding due to walls, ceiling and floor. On average, the value obtained for n in all cases at 28 GHz with the horn receiver antenna was 1.73, which is similar to the value reported in [10] when the first corner is at 37 m. The case reported in [10] only considered 2-D measurements at 28 GHz with a horn receiver antenna, where the RMSE for the similar indoor corridor was 2.7 dB. However, when the model (1) is employed for 3-D predictions the RMSE increases to 3.6 dB for the first case evaluated, where only the measurements obtained at h_2 are considered. The Kriging-aided model improves accuracy predicting path loss with 3.1 dB RMSE.

When comparing the second case with the first, an improvement is expected since the tuning data now includes power measurements at heights that correspond to those for which the model-predictions will be compared with measurements. However, when (1) is employed, the RMSEs remain essentially the same for both frequencies. Instead, when using Kriging, better accuracy is observed in virtually all cases.

All three cases allow us to validate the enhancement obtained when using the Kriging model instead of slope and intercept for 3-D predictions. The reduction in RMSE is clearly seen in Table I. For the third case, at 28 GHz, the RMSE indicates that with the horn receiver antenna there is an improvement of 17%, and a 31% with the omnidirectional when (2) is used to predict path loss. At 60 GHz, with the horn receiver antenna the RMSE decreases by 19%, and with the omnidirectional by 36% when using the Kriging-aided model. When the third case is tested considering all link configurations (both frequencies and receiver antennas), the advantage of Kriging is validated by employing only 60% of the measured data, providing an excellent tradeoff between the averaged accuracy and the number of tuning samples. We found the RMSE to be 2.4 dB using 95 tuning samples (from the 159 samples measured at the different heights).

Accurate 3-D coverage prediction of wireless links is an important consideration in assessing the quality of service. It follows from our results that the methodology here proposed for indoor corridors is a useful prediction tool to make effective use of a limited number of available measurements. Based on our extensive set of measurements and reviewing the results, we found that using only 60% of the data, the minimum prediction error of the Kriging-based model was up to 41% lower than that of the single-slope segmentwise model.

V. CONCLUSION

Careful and extensive measurements to obtain path loss after averaging small scale fades were collected using 28 and 60 GHz narrowband sounders in a long indoor corridor with break. We obtain a reliable 3-D Kriging-aided path loss model to plan and deploy mmWave wireless communication systems in indoor corridors, which effectively considers all the singularities and site-associated features that are implicit in measured samples.

ACKNOWLEDGMENT

The author M. E. Diago-Mosquera would like to thank the PUCV and USM during her doctoral stay, which allowed her to assess the outstanding results presented in this letter. The authors would like to thank A. R. Lopez, F. Torres, V. Díaz, and D. Orrego for all the help with the extensive measurement campaign, and Leonardo Guerrero for platforms improvements and his continuous support.

REFERENCES

[1] S. Ruiz et al., "5G and beyond networks," in *Inclusive Radio Communications for 5G and Beyond*. New York, NY, USA: Academic, 2021, ch. 6, pp. 141–186, doi: 10.1016/B978-0-12-820581-5.00012-2.

[2] S. Salous et al., "IRACON channel measurements and models," in *nclusive Radio Communications for 5G and Beyond*. Jan. 2021, ch. 3, pp. 49–105, doi: 10.1016/B978-0-12-820581-5.00009-2.

[3] D. Porrat and D. C. Cox, "UHF propagation in indoor hallways," *IEEE Trans. Wireless Commun.*, vol. 3, no. 4, pp. 1188–1198, Jul. 2004, doi: 10.1109/TWC.2004.828023.

[4] H. Xu, V. Kukshya, and T. S. Rappaport, "Spatial and temporal characteristics of 60-GHZ indoor channels," *IEEE J. Sel. Areas Commun.*, vol. 20, no. 3, pp. 620–630, Apr. 2002, doi: 10.1109/49.995521.

[5] N. O. Oyie and T. J. O. Afullo, "Measurements and analysis of large-scale path loss model at 14 and 22 GHz in indoor corridor," *IEEE Access*, vol. 6, pp. 17205–17214, 2018, doi: 10.1109/ACCESS.2018.2802038.

[6] T. S. Rappaport, *Wireless Communications—Principles And Practice*. New York, NY, USA: Prentice-Hall, 2002.

[7] X. Zhao, S. Geng, and B. M. Coulibaly, "Path-loss model including LOS-NLOS transition regions for indoor corridors at 5 GHz," *IEEE Antennas Propag. Mag.*, vol. 55, no. 3, pp. 217–223, Jun. 2013, doi: 10.1109/MAP.2013.6586668.

[8] I. D. S. Batalha et al., "Indoor corridor and office propagation measurements and channel models at 8, 9, 10 and 11 GHz," *IEEE Access*, vol. 7, pp. 55005–55021, 2019, doi: 10.1109/ACCESS.2019.2911866.

[9] H. A. Obeidat et al., "An indoor path loss prediction model using wall correction factors for wireless local area network and 5G indoor networks," *Radio Sci.*, vol. 53, no. 4, pp. 544–564, Apr. 2018, doi: 10.1002/2018RS006536.

[10] D. Chizhik, J. Du, R. Feick, M. Rodriguez, G. Castro, and R. A. Valenzuela, "Path loss and directional gain measurements at 28 GHz for non-line-of-sight coverage of indoors with corridors," *IEEE Trans. Antennas Propag.*, vol. 68, no. 6, pp. 4820–4830, Jun. 2020, doi: 10.1109/TAP.2020.2972609.

[11] F. D. Diba, M. A. Samad, and D. Y. Choi, "Centimeter and millimeter-wave propagation characteristics for indoor corridors: Results from measurements and models," *IEEE Access*, vol. 9, pp. 158726–158737, 2021, doi: 10.1109/ACCESS.2021.3130293.

[12] M. K. Elmezughi and T. J. Afullo, "An efficient approach of improving path loss models for future mobile networks in enclosed indoor environments," *IEEE Access*, vol. 9, pp. 110332–110345, 2021, doi: 10.1109/ACCESS.2021.3102991.

[13] Y. Shen, Y. Shao, L. Xi, H. Zhang, and J. Zhang, "Millimeter-Wave propagation measurement and modeling in indoor corridor and stairwell at 26 and 38 GHz," *IEEE Access*, vol. 9, pp. 87792–87805, 2021, doi: 10.1109/ACCESS.2021.3081822.

[14] H.-S. Jo, C. Park, E. Lee, H. K. Choi, and J. Park, "Path loss prediction based on machine learning techniques: Principal component analysis, artificial neural network, and Gaussian process," *Sensors*, vol. 20, no. 7, Mar. 2020, Art. no. 1927, doi: 10.3390/s20071927.

[15] K. Sato, K. Suto, K. Inage, K. Adachi, and T. Fujii, "Space-frequency-interpolated radio map," *IEEE Trans. Veh. Technol.*, vol. 70, no. 1, pp. 714–725, Jan. 2021, doi: 10.1109/TVT.2021.3049894.

[16] M. E. Diago-Mosquera, A. Aragon-Zavala, L. Azpilicueta, R. Shubair, and F. Falcone, "A 3D indoor analysis of path loss modeling using Kriging techniques," *IEEE Antennas Wireless Propag. Lett.*, vol. 21, no. 6, pp. 1218–1222, Jun. 2022, doi: 10.1109/LAWP.2022.3162160.

[17] M. E. Diago-Mosquera, A. Aragón-Zavala, and M. Rodriguez, "Testing a 5G communication system: Kriging-aided O2I path loss modeling based on 3.5 GHz measurement analysis," *Sensors*, vol. 21, no. 20, Oct. 2021, Art. no. 6716, doi: 10.3390/S21206716.

[18] M. E. Diago-Mosquera, A. Aragón-Zavala, and C. Vargas-Rosales, "The performance of in-building measurement-based path loss modelling using Kriging," *Microw., Antennas Propag.*, vol. 15, Jun. 2021, Art. no. mia2.12163, doi: 10.1049/mia2.12163.

[19] M. E. Diago-Mosquera, A. Aragon-Zavala, F. A. Rodriguez-Corbo, M. Celaya-Echarri, R. Shubair, and L. Azpilicueta, "Tuning selection impact on Kriging-aided in-building path loss modeling," *IEEE Antennas Wireless Propag. Lett.*, vol. 21, no. 1, pp. 84–88, Jan. 2022, doi: 10.1109/LAWP.2021.3118673.

[20] K. Sato, K. Inage, and T. Fujii, "Radio environment map construction with joint space-frequency interpolation," in *Proc. Int. Conf. Artif. Intell. Inf. Commun.*, Feb. 2020, pp. 051–054, doi: 10.1109/ICAIIC48513.2020.9065217.

[21] A. Konak, "Estimating path loss in wireless local area networks using ordinary Kriging," in *Proc. Winter Simul. Conf.*, 2010, pp. 2888–2896, doi: 10.1109/WSC.2010.5678983.

[22] M. H. Trauth, "Spatial data," in *MATLAB Recipes for Earth Sciences*, 4th ed. Berlin, Germany: Springer, 2015, pp. 1–427.